

Preflight Summary Report for: jacs.7b07619.pdf

Profile: Digital printing (B/W) (Processed pages 1 to 11)

Processed by Jennifer Schomaker, Date: 4/22/2018 11:44 AM

Fixups

-  Set minimum line width to 0.14 pt (105 objects)
-  Downsample grayscale images to 300 ppi if above 450 ppi (2 objects)
-  Compress all uncompressed objects using lossless ZIP compression (1 object)
-  Recompress LZW as ZIP (1 object)
-  Convert color to B/W (25874 objects)
-  Convert registration color to CMYK black only (88 objects)

Results (Summary)

-  No problems found

Document information

File name: "jacs.7b07619.pdf"
Path: "C:\Users\Jennifer Schomaker\Desktop\NSF Silver Progress reports"
PDF version number: "1.3"
File size (MB): 1.6
Title: "Inverting Steric Effects: Using "Attractive" Noncovalent Interactions To Direct Silver-Catalyzed Nitrene Transfer"
Author: "Minxue Huang, Tzuhsing Yang, Jonathan D. Paretsky, John F. Berry, and Jennifer M. Schomaker"
Creator: "Arbortext Advanced Print Publisher 10.0.1465/W Unicode"
Producer: "Acrobat Distiller 8.1.0 (Windows); modified using iText 4.2.0 by 1T3XT"
Created: "11/29/2017 1:07 PM"
Modified: "4/22/2018 11:44 AM"
Subject: "J. Am. Chem. Soc. 2017.139:17376-17386"
Trapping: "Unknown"
Number of plates: 1
Names of plates: "(Black)"

Environment

Preflight, 18.2.0 (201)
Acrobat version: 18.110
Operating system: Microsoft Windows 7 Service Pack 1 (Build 7601)

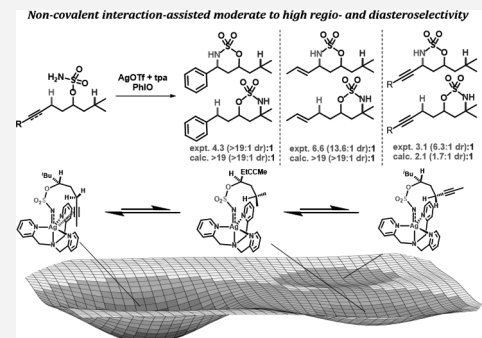
Inverting Steric Effects: Using “Attractive” Noncovalent Interactions To Direct Silver-Catalyzed Nitrene Transfer

Minxue Huang,[†] Tzuhsiu Yang,[†] Jonathan D. Paretsky, John F. Berry,^{*ID} and Jennifer M. Schomaker^{*ID}

Department of Chemistry, University of Wisconsin, Madison, Wisconsin 53706, United States

Supporting Information

ABSTRACT: Nitrene transfer (NT) reactions represent powerful and direct methods to convert C–H bonds into amine groups that are prevalent in many commodity chemicals and pharmaceuticals. The importance of the C–N bond has stimulated the development of numerous transition-metal complexes to effect chemo-, regio-, and diastereoselective NT. An ongoing challenge is to understand how subtle interactions between catalyst and substrate influence the site-selectivity of the C–H amination event. In this work, we explore the underlying reasons why Ag(tpa)OTf (tpa = tris(pyridylmethyl)amine) prefers to activate α -conjugated C–H bonds over 3° alkyl C(sp³)–H bonds and apply these insights to reaction optimization and catalyst design. Experimental results suggest possible roles of noncovalent interactions (NCIs) in directing the NT; computational studies support the involvement of $\pi \cdots \pi$ and Ag $\cdots \pi$ interactions between catalyst and substrate, primarily by lowering the energy of the directed transition state and reaction conformers. A simple Hess’s law relationship can be employed to predict selectivities for new substrates containing competing NCIs. The insights presented herein are poised to inspire the design of other catalyst-controlled C–H functionalization reactions.



INTRODUCTION

Strategies for the selective functionalization of C–H bonds can be grouped into two broad categories, consisting of directed and nondirected reactions. The former approach relies on the association of a substrate to a metal center, typically through a polar functional group, to facilitate the activation of a specific proximal C–H bond (Figure 1A).¹ In contrast, nondirected strategies generate transient and highly reactive metal-containing intermediates; these engage with C–H bonds largely based on inherent steric and electronic preferences dictated by the substrate.² Group-transfer reactions, including metal-catalyzed nitrene transfer reactions (NT), have traditionally fallen into the latter category (Figure 1B).

Transition-metal-catalyzed NT represents a convenient method for directly transforming C–H bonds to valuable C–N bonds.^{3–11} Recent progress in C–H amination via NT has focused mainly on situations where individual C–H bonds display reasonable differences in terms of their intrinsic electronic, steric, or stereoelectronic features.¹² In these scenarios, *repulsive* noncovalent interactions (NCIs) between the catalyst and substrate are used to alter the selectivity of the reaction (Figure 1C).¹³ A complementary, but underexplored, approach is to build *attractive* NCIs into a substrate/catalyst combination (Figure 1D).¹⁴ As an example, hydrogen-bonding between a porphyrin-supported Co catalyst and a nitrene generated from PhSO₂N₃ has been demonstrated by Zhang and de Bruin to accelerate the rate of olefin aziridination.¹⁵ In effect, this strategy enables the NT event to be ‘directed’ via a NCI; however, to our knowledge, the fundamental question of

whether the inherent selectivity of C–H functionalization proceeding through NT can be enhanced or overridden through attractive, noncovalent interactions has not been explicitly addressed.

Of the transition metals that catalyze NT,^{4–11} we selected Ag(I) complexes to study directed amination due to their diverse coordination environments,^{16,17} Lewis acidity, and ability to engage in cation– π interactions. Substrates adorned with traditional directing groups, such as pyridines and imines, proved unsuccessful, as strong interactions between Ag and directing groups precluded our ability to tune the site of the C–H amination. This led us to consider whether weak attractive NCIs between catalyst and substrate might constitute a more viable design principle to achieve flexible and tunable directed C–H amination. Herein, we report experimental and computational studies supporting the ability of NCIs, including Ag $\cdots \pi$ and aromatic–aromatic interactions, to influence the outcome of NT reactions.

Computational modeling of NCIs is particularly challenging for current quantum chemical methods.¹⁸ The need to sample multiple conformations and configurations of the reactants and transition states is not straightforward, although for simple systems, this can be dealt with using molecular dynamics simulations.¹⁹ However, for the large Ag complexes studied herein, the use of molecular dynamics is not possible. We have therefore adopted a statistical mechanics approach where the

Received: July 20, 2017

Published: November 1, 2017



ACS Publications

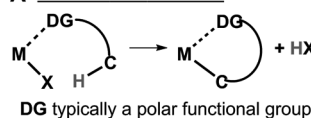
© 2017 American Chemical Society

17376

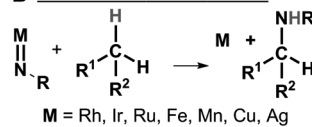
DOI: 10.1021/jacs.7b07619
J. Am. Chem. Soc. 2017, 139, 17376–17386

Previous work:

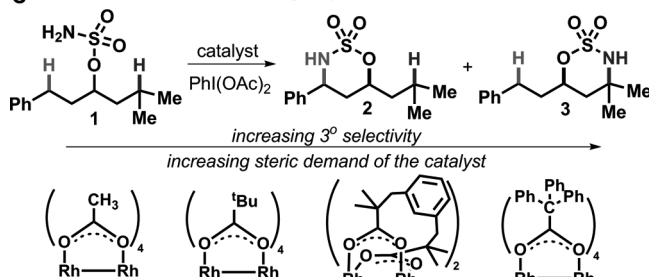
A Directed C–H activation



B Non-directed nitrene transfer



C Selective nitrene transfer through repulsive non-covalent interactions



This work:

D Directed nitrene transfer through attractive non-covalent interactions

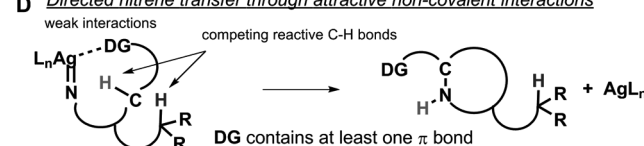


Figure 1. General strategies for C–H functionalization.

weighted populations of the key conformations of the catalyst are taken into account and used to calculate product distributions. The insights drawn from these computational studies were implemented in the design of second-generation Ag catalysts with improved preference for the amination of electron-poor benzylic C–H and other α -conjugated C–H bonds, paving the way for new catalysts that effectively harness NCIs to drive selectivity in metal-catalyzed group transfers.

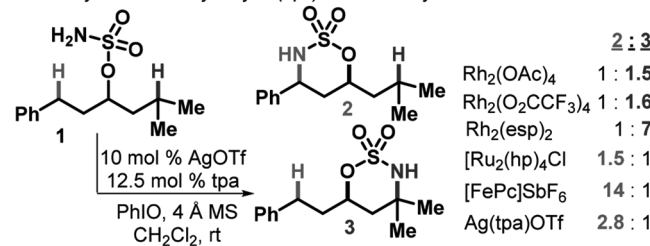
■ RESULTS AND DISCUSSION

We recently reported that Ag(tpa)OTf, a silver complex supported by a tris(2-pyridylmethyl)amine (tpa) ligand, unexpectedly preferred to aminate α -conjugated C–H bonds over 3° alkyl $C(sp^3)$ –H bonds, albeit in moderate selectivities.^{17a} Further optimization yielded several observations relevant to a deeper understanding of the mechanism of intramolecular NT promoted by Ag(tpa)OTf, including the possibility that $\pi\cdots\pi$ or Ag…π interactions play important roles in directing selectivity.

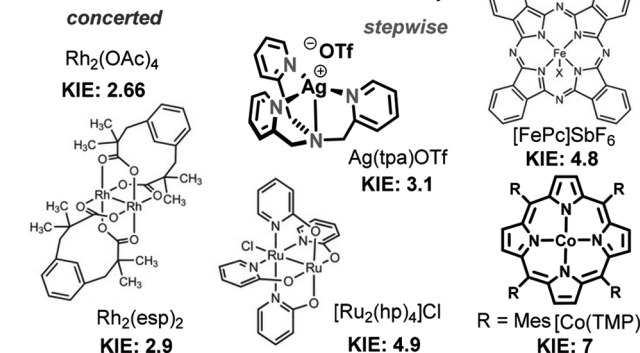
Mechanistic Aspects. The first indication that Ag(tpa)OTf might induce site-selective NT through directing NCIs arose from studies comparing its reactivity with other known NT catalysts. Reactions of **1** (Scheme 1A) with $Rh(II)_2L_n$ displayed higher selectivities for **3** as the bridging equatorial ligands on the Rh increased in size.¹³ This trend of catalyst-controlled selectivity falls within the paradigm of steric-driven regioselectivity, where the α -phenyl ring of **1** displays greater steric repulsion with the equatorial ligands than the two geminal α -methyl groups during the abstraction of the γ C–H bond (cf. the cone angle of 145° for $PPPh_3$ vs 118° for $P(CH_3)_3$). On the other hand, Ru and Fe catalysts furnished **2** with varying degrees of selectivity.^{8c,20} These results fit the prevailing NT mechanistic paradigm, where catalysts proceeding via stepwise H-transfer/radical recombination (S-HT:RR) tend to show higher kinetic isotope effect (KIE) values (Scheme 1B) and favor amination of weaker C–H bonds (BDE: 2° benzylic C–H \sim 85 kcal/mol; 3° alkyl $C(sp^3)$ –H \sim 95 kcal/mol).

Scheme 1. Comparison of Metal-Catalyzed Nitrene Transfers

A. benzylic vs. tertiary alkyl $C(sp^3)$ –H selectivity



B. KIE values for selected nitrene transfer catalysts



However, the range of site-selectivities described in Scheme 1A is curious, suggesting that invoking “stepwise vs concerted” mechanisms to explain the observed results does not sufficiently capture subtle interactions that might shape the outcome of the C–H amination.

Ag(tpa)OTf proved an intriguing catalyst for NT; typical mechanistic probes, including KIE and radical clock studies (Scheme 1B), initially appeared to indicate a concerted pathway, similar to $Rh(II)_2L_n$ catalysis.¹³ However, computational studies carried out by Berry and Musaev showed that a requirement for concerted nitrene transfer is the presence of an empty N-centered orbital on the metal–nitrene intermediate.²¹ The triplet ground states of Ag–nitrene intermediates do not permit this condition to be met; thus, reactions catalyzed by Ag(tpa)OTf are electronically prohibited from occurring via concerted pathways. Further computational modeling resolved this discrepancy by showing that Ag-catalyzed NT can proceed via a mechanism we have termed “elementary hydrogen transfer/radical recombination” (E-HT:RR). This mechanism occurs with a single HT transition state, followed by a radical recombination step displaying no energy barrier; radical species are not stationary points on the potential energy surface.^{17e}

In addition to comparisons of the KIE and site-selectivity of metal catalysts for NT (Scheme 1), Hammett studies were carried out with Ag(tpa)OTf (Figure S-1, Supporting Information), giving $\rho = -0.687 \pm 0.024$ using σ^* parameters.²² As with all metal-catalyzed NT reactions reported to date, the negative ρ value indicates a buildup of positive charge in the transition state (TS).^{13,17a,20} These results imply an earlier TS for reactions catalyzed by Ag(tpa)OTf, as compared to other catalysts proceeding via stepwise NT; however, the exact reasons for these mechanistic differences are currently unclear.^{17e}

Interestingly, examination of KIE and Hammett ρ values showed similarities between Ag(tpa)OTf and Rh_2L_n (Scheme 1B),^{13,17a} yet the selectivity of the former was more reminiscent of the results noted with Ru, Fe, and Co complexes.^{8c,20,23}

While this might be attributed to stepwise NT promoted by Fe, Ru, Co, and Ag, we considered the possibility that additional factors might be responsible for the behavior observed with Ag(tpa)OTf. For example, previous studies found that Ag(I) complexes supported by N-donor ligands show highly fluxional behavior in solution, depending on the counteranion and ligand identity.^{17g} This dynamic behavior was particularly evident in Ag(tpa)OTf, which may enable it to engage in $\pi\cdots\pi$ and Ag $\cdots\pi$ interactions.

Attractive NCIs between aromatic rings have long been known to play important structural roles in molecular recognition, template-directed synthesis, protein folding, and many other key biological processes.²⁴ The prototypical benzene dimer $\pi\cdots\pi$ stacking interaction is on the order of 2–3 kcal/mol, with the two most stable conformations preferring T-shaped or parallel-displaced orientations.²⁵ In particular, a parallel-displaced orientation between an aryl group of a NT substrate and a pyridyl ring of Ag(tpa)OTf could yield donor–acceptor interactions that effectively stabilize a transition state leading to benzylic C–H amination.²⁶ In the context of Ag $\cdots\pi$ interactions, the aryl group of **1** (Scheme 1A) could engage with silver to direct the outcome of the NT event. Indeed, there are numerous examples of complexes containing Ag $\cdots\pi$ interactions in the solid state; however, to our knowledge, such interactions have not been invoked to control selectivity in Ag-catalyzed group transfer reactions.^{14g,h,27}

Experimental Probes of Noncovalent Interactions. NCIs are often sensitive to reaction conditions; thus, studies to assess the impact of the Ag counteranion, solvent, temperature, and concentration on the amination of **1** were carried out (Table S-1, SI). The effect of the counteranion on selectivity was minimal, suggesting it is not bound to Ag during the key bond-forming event.^{17e,f,21} Counteranion-free Ag-nitrene species were also supported by computational studies (vide infra).^{17e,i} Concentration had little effect on selectivity, while decreasing the temperature from +25 to $-20\text{ }^\circ\text{C}$ improved the 2:3 ratio. A range of aprotic solvents were examined with **1** (Table 1) at $25\text{ }^\circ\text{C}$; the selectivity for 2:3 correlated with solvent polarity (Table S-2, SI). Overall yields of **2** and **3** were

Table 1. Relationship between 2:3 and Reichardt E_T^N Values

entry	solvent	E_T^N	2 : 3 ^b	yield (2+3+Im) ^c
1	CCl ₄	0.052	5.8 : 1	86%
2	p-xylene	0.074	5.1 : 1	95%
3	toluene	0.099	4.8 : 1	92%
4	benzene	0.111	4.5 : 1	>99%
5	Et ₂ O ^d	0.117	3.8 : 1	51% (~49% 1)
6	PhCl	0.188	4.2 : 1	89%
7	EtOAc	0.228	3.1 : 1	94%
8	PhCF ₃ ^d	0.241	3.8 : 1	91%
9	CHCl ₃	0.259	3.5 : 1	90%
10	CH ₂ Cl ₂	0.309	2.8 : 1	91%
11	(CH ₂) ₂ Cl ₂	0.327	2.5 : 1	91%
12	MeCN	0.460	2.2 : 1	79%

^a10 mol % of Ag(tpa)OTf, 3.5 equiv of PhIO, 4 Å MS, solvent, 0.05 M, rt, 2 h. ^bAverage of two trials; imine formed is considered in the ratios. ^cIm is the imine formed from overoxidation of **2**. ^dAverage of three trials.

excellent in most cases, as was the dr of **2** ($>19:1$ in all cases). Preference for benzylic amination tracked best with Reichardt E_T^N values, as opposed to other measures of solvent polarity, including dipole moment and dielectric constant.^{25,28} E_T^N values are derived by measuring the long-wave UV–vis absorption band of a negative solvachromatic pyridinium N-phenoxide betaine dye in the solvent of interest.²⁹

As previously mentioned, the NCIs most likely to influence the preference for benzylic C–H amination with Ag(tpa)OTf are 1) $\pi\cdots\pi$ interactions between one of the pyridine ligand arms and the aryl group of **1** or **2**) Ag $\cdots\pi$ interactions between Ag and **1**. In the former case, the strength of the $\pi\cdots\pi$ interactions is largely influenced by electrostatic attractions between the two aromatic rings or by solvation/desolvation (solvophobic) effects.^{28,30} In the aprotic and nonpolar solvents employed for our chemistry, electrostatic interactions should dominate, with the strength of the $\pi\cdots\pi$ interaction increasing as solvent polarity decreases.^{28,30,31} This is observed experimentally in moving from less polar solvents, such as CCl₄ (Table 1, entry 1), to solvents of increasing E_T^N such as benzene, PhCF₃, and CHCl₃ (entries 4, 8, and 9). However, if Ag $\cdots\pi$ interactions are invoked as the primary NCI-controlling preference for benzylic C–H amination, sufficient space around the Ag must be available to accommodate engagement of the substrate with the metal. Based on our knowledge of solution-state structures of Ag(tpa)OTf, this is unlikely when the π donor is a large aryl group; however, such interactions may play a significant role in substrates with less sterically demanding π donors, such as alkenes and alkynes (vide infra).^{17g}

Experimental Evidence Suggesting NCIs Play Roles in Selective NT into Benzylic C–H Bonds. Given that solvent effects influence the effectiveness of NCIs, we were curious if the preference for reaction at the benzylic C–H bond of **7–10** could be improved, compared to previous results in CH₂Cl₂ (parentheses in Table 2).^{17a} While 1:1 CHCl₃:PhCF₃ gave the

Table 2. Selectivity for NT in Competing 2° Benzylic vs 3° Alkyl C(sp³)–H Bond Aminations with Ag(tpa)OTf

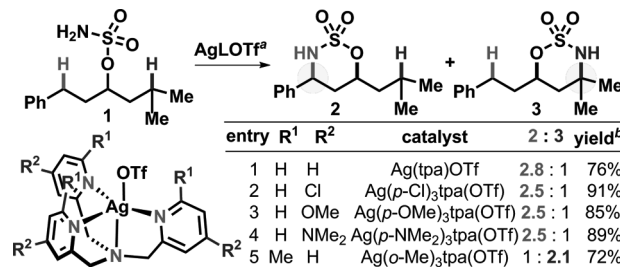
^a10 mol % of Ag(tpa)OTf formed by combining 10 mol % of AgOTf and 12.5 mol % of tpa. ^bPrevious results in CH₂Cl₂ at rt are shown in parentheses.

highest selectivity for **2** at $-20\text{ }^\circ\text{C}$ (Table S-1, entry 9), CHCl₃ was adopted for further study. Preference for benzylic C–H amination increased with our new conditions when sterics of the 3° alkyl C(sp³)–H bond were not overly demanding. Sulfamates **1** and **7–9** showed improved selectivity for **2** and **7a–9a**, respectively, in $>19:1$ dr favoring the *syn* product. Large alkyl substituents, such as the diisopropyl group of **10**, gave only benzylic amination, indicating a steric component largely independent of solvent. Although selectivity gains are modest, they do represent $>10\%$ increases in yield, render purification

of product mixtures easier and support the possibility of $\pi\cdots\pi$ interactions between the tpa ligand and the substrate aryl group.

The lower C–H BDEs of benzylic C–H (~82–83 kcal/mol) vs 3° alkyl C(sp³)–H bonds (~95 kcal/mol) could also explain the improved selectivities in Table 2. As Ag-catalyzed NT is stepwise in nature, preferential reaction at the weaker C–H bond might be expected.^{17e} However, evidence that BDE is not the primary determinant of site-selectivity is shown by minimal changes to 2:3 as the electronics of the tpa ligand are modified (Scheme 2, entries 1–4). In contrast, preference for 3 using

Scheme 2. Ligand Identity Influences Site-Selectivity



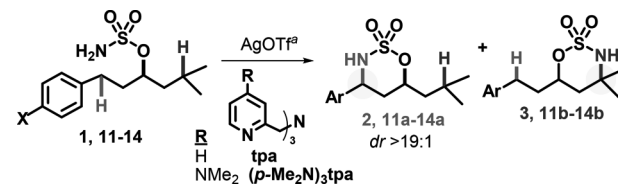
^a10 mol % of catalyst, 3.5 equiv of PhIO, 4 Å MS, 0.05 M CH₂Cl₂.
^bIsolated yields.

Ag(o-Me)₃tpa(OTf) (entry 5) is due to changes in the preferred conformation of the active catalyst, likely preventing the presence of NCIs between the substrate and catalyst.^{17g}

Testing the Possibility of Directing $\pi\cdots\pi$ Interactions in NT Reactions through Modified tpa Ligands. To test if $\pi\cdots\pi$ interactions drive a preference for benzylic C–H amination, ligand/substrate combinations were designed to amplify these proposed NCIs. Tpa ligands with electron-donating or -withdrawing groups were prepared, as exemplified by (p-Me₂N)₃tpa, (p-MeO)₃tpa, and (p-Cl)₃tpa (see the SI for details). The performance of Ag(tpa)OTf was benchmarked in entries 1–3 (Table 3), showing that the 2:3 ratio increased from 2.8:1 to 4.3:1 in moving from CH₂Cl₂ to CHCl₃ at –20 °C. Data for CHCl₃ could not be collected at rt due to formation of the N-chloramine of 2. Interestingly, an increase in selectivity was not noted with Ag(p-Me₂N)₃tpa(OTf) (entries 4–6); in fact, the reaction rate decreased in CHCl₃ (entry 6). Based on our previous studies of the dynamic behavior of Ag(I) complexes in solution,^{17g} we propose that a shift in dynamic equilibrium favors tetradentate binding of (p-Me₂N)₃tpa to Ag, in contrast to the largely tridentate binding preferred by the parent tpa ligand. The electron-rich nature of (p-Me₂N)₃tpa, coupled with the decreased fluxionality of Ag(p-Me₂N)₃tpa(OTf) at –20 °C in CHCl₃, results in little change in the 2:3 ratio when Ag(tpa)OTf is substituted with Ag(p-Me₂N)₃tpa(OTf). This fits the argument that $\pi\cdots\pi$ interactions play a role in controlling selectivity, as a more electron-rich ligand would not result in increased NCIs with the Ph substituent of 1. On the basis of this analysis, Ag(p-Me₂N)₃tpa(OTf) was not explored with electron-rich 11 and 12; rather, changes to the solvent and temperature with Ag(tpa)OTf were adequate to give excellent selectivities for 11a and 12a (entries 7–10).

Key results supporting $\pi\cdots\pi$ interactions as a viable catalyst design strategy were obtained when substrate and catalyst combinations maximized the impact of NCIs. The presence of electron-poor groups on the aryl moiety of 13 and 14 (entries 11–16) did increase selectivity for 13a and 14a with

Table 3. Effect of Ligand Identity on the Selectivity for 2° Benzylic C–H vs 3° Alkyl C(sp³)–H Bond Amination



entry	X	ligand	solvent	temp	2:3 or a:b	yield
1	H	tpa	CH ₂ Cl ₂	rt	2.8:1 2:3	76%
2	H	tpa	CH ₂ Cl ₂	–20 °C	3.5:1 2:3	94%
3	H	tpa	CHCl ₃	–20 °C	4.3:1 2:3	92%
4	H	(p-Me ₂ N) ₃ tpa	CH ₂ Cl ₂	rt	2.5:1 2:3	89% ^b
5	H	(p-Me ₂ N) ₃ tpa	CH ₂ Cl ₂	–20 °C	2.8:1 2:3	87% ^b
6	H	(p-Me ₂ N) ₃ tpa	CHCl ₃	–20 °C	2.7:1 2:3	37% ^{b,c}
7	OMe	tpa	CH ₂ Cl ₂	rt	4.7:1 11a:b	85%
8	OMe	tpa	CHCl ₃	–20 °C	>19:1 11a:b	84%
9	Me	tpa	CH ₂ Cl ₂	rt	4.4:1 12a:b	81%
10	Me	tpa	CHCl ₃	–20 °C	8.8:1 12a:b	89%
11	Br	tpa	CH ₂ Cl ₂	rt	1.8:1 13a:b	88%
12	Br	tpa	CHCl ₃	–20 °C	3.6:1 13a:b	84%
13	Br	(p-Me ₂ N) ₃ tpa	CH ₂ Cl ₂	–20 °C	7.1:1 13a:b	83%
14	CF ₃	tpa	CH ₂ Cl ₂	rt	1:1.3 14a:b	96%
15	CF ₃	tpa	CHCl ₃	–20 °C	1.4:1 14a:b	92%
16	CF ₃	(p-Me ₂ N) ₃ tpa	CH ₂ Cl ₂	–20 °C	2.6:1 14a:b	86%

^a10 mol % of AgOTf, 12.5 mol % of ligand, 3.5 equiv of PhIO, 4 Å MS, rt or –20 °C, 2 h. ^bNMR yield, PhSiMe₃ internal standard. ^c51% recovered 1.

Ag(tpa)OTf (compare entries 11 with 12 and 14 with 15); however, this effect was more pronounced with Ag(p-Me₂N)₃tpa(OTf) (entries 13, 16). The 13a:b ratio improved from 3.6:1 using Ag(tpa)OTf to 7.1:1 with Ag(p-Me₂N)₃tpa(OTf) in comparable yields and dr, favoring the *syn* product (compare entries 12–13). Substrate 14, with a CF₃ group on the aryl ring, also displayed improved 14a:b ratios from 1.4:1 with Ag(tpa)OTf to 2.6:1 with Ag(p-Me₂N)₃tpa(OTf) (compare entries 15–16). Increased benzylic C–H amination of 14 with Ag(p-Me₂N)₃tpa(OTf) is further corroborated by qualitative reproduction of the experimental results by density functional theory (DFT). Changing the ligand from tpa to (p-Me₂N)₃tpa resulted in an increase of 1.5 kcal·mol^{–1} in the solvation- and dispersion-corrected electronic driving force ($\Delta\Delta E_{\text{solv},D_3}$) for the benzylic *pro-(R)* C–H bond using partially relaxed models. The role of NCIs in driving regioselectivity and dr is discussed from a theoretical perspective later in the paper.

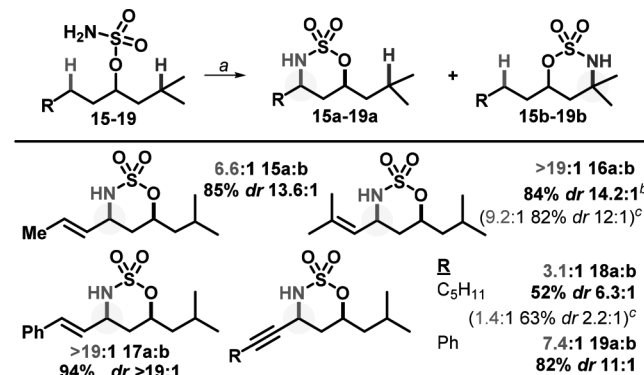
Another explanation for the increased preference for electron-poor benzylic C–H bonds over competing 3° alkyl C(sp³)–H bonds in 13 and 14 is the stabilization of the putative Ag-nitrene by the electron-rich (Me₂N)₃tpa ligand. This would render the Ag nitrene more radical-like and potentially more selective. Increased radical-like character might be reflected in the KIE for the reaction; however, comparison of KIEs for Ag(tpa)OTf and Ag(p-Me₂N)₃tpa(OTf) showed no difference within experimental error.

Experimental Evidence Suggesting a Role for NCIs in the Preferred Selectivity for NT into Allylic and Propargylic C–H Bonds. We next turned our attention to explaining the preference for amination of allylic and propargylic C–H over 3° alkyl C(sp³)–H bonds. Ag $\cdots\pi$ interactions involving acyclic π bonds are well-known;²⁷ interactions between a silver cation and ethene were first described by Dewar as long ago as 1951.^{27a} Similar to $\pi\cdots\pi$

interactions, $\text{Ag}\cdots\pi$ interactions are relatively weak, at approximately 1–3 kcal/mol of energetic stabilization.³²

The possibility of directing $\text{Ag}\cdots\pi$ NCIs via the π -donor capability of alkenes and alkynes was investigated through competitive NT comparing the reactivity of allylic and propargylic C–H bonds vs 3° alkyl C(sp³)–H bonds (Table 4). In alkenes 11–13, good chemo- and site-selectivities for

Table 4. NT Selectivity in Competing 2° Allylic and Propargylic C–H vs 3° Alkyl C(sp³)–H Bond Aminations with Ag(tpa)OTf



^a 10 mol % of AgOTf, 12.5 mol % of tpa, 3.5 equiv of PhIO, 0.05 M CHCl₃, 4 Å MS, –20 °C. ^b 5% rearranged aziridine. ^c Previous conditions using CH₂C₁ at rt.

allylic C–H amination gave 15a–17a with high *syn* dr. Similar to Table 2, the lower C–H BDE of allylic C–H (~82–83 kcal/mol) vs competing 3° alkyl C(sp³)–H bonds (~95 kcal/mol) may impact reaction outcome. However, we were surprised to find that the preference for amination of propargylic C–H bonds in 18 and 19 was lower than expected, despite decreased sterics and similar BDE (~85 kcal/mol) to allylic and benzylic C–H bonds. These unexpected results were explored through computational studies, as described in the next section.

Computational Modeling of Multiple Catalyst Conformations in Silver-Catalyzed Intramolecular Nitrene Transfer (NT). Exploiting NCIs for catalyst-controlled, site-selective NT is challenging, as these interactions are weak compared to covalent bonds. In addition, multiple conformations with similar energies may be accessible within a targeted catalyst structure. The prediction of major conformations based on conceptually designed catalyst structures are aided by quantum-chemical methods, where DFT can examine the presence of NCIs in the context of both catalyst design and the physical understanding of catalysis.¹⁴ One caveat to computational design or rationalization of NCIs in known catalysts is that DFT cannot describe important long-range electron correlation.^{18a–c} Such correlation can be recovered by (1) including a fixed amount of Hartree–Fock exchange (HFX) in the density functional to give global hybrid functionals such as the popular B3LYP, used in this study for geometry optimizations and frequency calculations, or (2) using a variable amount of HFX to give a range-separated hybrid functional such as *w*B97X, used in this study for single-point energies.³³ Empirical corrections, such as DFT-D3 used in this study, further improve the recovery of long-range correlation.^{18d} We use these methods here to make structural and energetic models of NCIs between catalysts and substrates at the level of DFT.

The weak nature of NCIs means that both nondirected and directed conformations of the catalyst–substrate complex are present and catalytically relevant. In the calculations presented herein, the reactive nitrene intermediate (denoted RC) exists in two conformations, one predisposed for benzylic amination and the other for reaction at the 3° C–H bond. Considering the general case of a catalyst with conformations RC_A and RC_B, there are two limiting cases for how these conformations contribute to the product distributions P_A and P_B, derived from RC_A and RC_B, respectively. In one case, the reaction is under kinetic control, while the other situation is best described by a Curtin–Hammett situation. In our computational work, the product ratios are calculated under both scenarios to assess whether selectivity of the NT occurs under kinetic-only or Curtin–Hammett-corrected control (see the SI for further details of these models).

Modeling NCIs from Ag(tpa)OTf–nitrene Species to C–H Amination Transition States. To better understand site-selectivity in competing reaction of benzylic vs 3° alkyl C(sp³)–H bonds (Table 1), DFT studies were performed on *pro*-benzylic and *pro*-3° conformers of potential Ag–nitrene intermediates, based on the structure of Ag(OTf)tpa. As counteranion identity has little effect, we focused on *pro*-benzylic counteranion-free [Ag(nitrene)tpa]⁺ (RC-1A) and [Ag(nitrene)(η ³-tpa)]⁺ complex (RC-1B) with one pyridyl arm detached (nitrene = NSO₃-(S)-CH(ⁱBu)(EtPh)), as VT-¹H NMR studies of Ag(tpa)OTf show hemilability of the ligand (Figure 2, Figure S-2 for 1C,D).^{17g,j} RC-1A is 12.9 kcal-

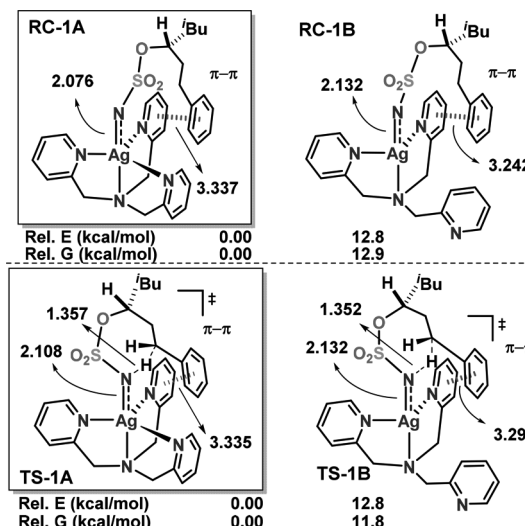


Figure 2. Reactant (top) and benzylic transition-state complexes (bottom) of 1A–1B (nitrene = NSO₃-(S)-CH(ⁱBu)(EtPh)). Distances are in angstroms. Relative single-point and Gibbs free energies are in kcal·mol^{–1}.

mol^{–1} more stable than RC-1B; consistent with previous work, the triplet is the lowest energy state for both structures, with the Ag–nitrene interaction showing partial σ and π bond character.^{17e} Ag–nitrene reactant complexes (RCs) are best described as Ag(II)–nitrene^{•–} (nitrene^{•–} = nitrene radical anion) structures. For all possible Ag–nitrene structures, critical points along the triplet potential surface (³PES) were scanned, and the transition states (TS) for either benzylic (both R and S products are considered) or 3° C–H amination were located. In total, 12 RC and TS structures were investigated:

the *pro*-benzylic and *pro*-3° RCs **1A–D** and *R*-benzylic, *S*-benzylic, and 3° TSs **1A–D**. Importantly, we found substrate-aryl···tpa-pyridyl π···π interactions between 3.22 and 3.34 Å in RCs:TSs for both **1A** and **1B**. No such π···π interaction occur in the *pro*-3° structures (**1C**, Figure S-2).

All reactant complexes (RC) perform nitrene insertion through an initial H-atom abstraction TS having a near-linear C···H···N structure (160–177°). Comparing the TS energies required to abstract either a benzylic (**Bn**) or 3° (T) C–H bond of the substrate in **1A–B**, we found the computed **Bn**:T selectivities to be >20:1 and 6.9:1, respectively. In contrast, **1A** and **1B** gave a computed **Bn**:T selectivity of 1:20, which does not match the experimental **Bn**:T ratio of 4.3:1.

To investigate potential Ag···π NCIs in alkenes, we computed the regioselectivity between an allylic C–H and a 3° C–H bond in **2A–D** (Figure 3). These structures are

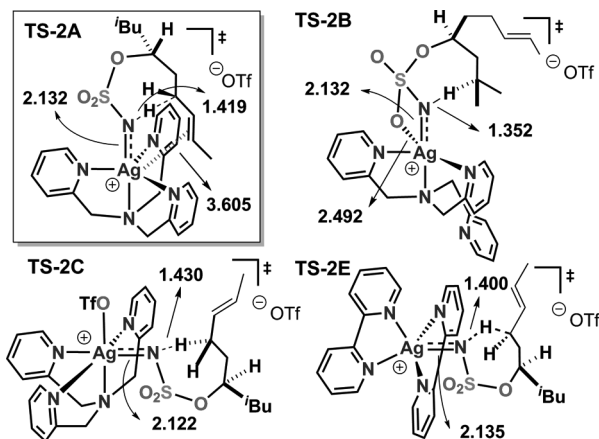


Figure 3. Lowest energy structures of Ag–nitrene transition-state complexes (nitrene = $\text{NSO}_3\text{-}(S)\text{-CH}(\text{iBu})(\text{Et-}(E)\text{-CH} = \text{CHMe})$): TS-2A–C and E. Distances are shown in Å.

analogous to **1A–D**, where the nitrene = $\text{NSO}_3\text{-}(S)\text{-CH}(\text{iBu})(\text{Et-}(E)\text{-CH} = \text{CHMe})$. As expected, calculations using model **2C** poorly predict selectivity for the 3° over the allylic (Al) C–H bond (calcd T:Al = > 20:1, *syn:anti* = 1:>20). In contrast, OTf-free *pro*-(S) **2A** and **2B** show potential Ag–olefin interactions (Ag···C distances from 3.52 to 3.60 Å). Calculations on **2A** gave Al:T = >20:1 and *syn:anti* = >20:1, which compare well with experiment, Al:T = 6.6:1 and *syn:anti* = 13.6:1. Preferential activation of the allylic C–H bond in **2A** likely results from an NCI between the Ag cation and the allylic π system. This type of Ag···π interaction is well-documented; in fact, 251 crystal structures of Ag–olefin complexes have been reported.³⁴

The results for **2B** were at first puzzling, as directing Ag–π interactions were expected to be present based on results observed for **2A**. However, the calculated (T:Al = >20:1 and *syn:anti* = 1:4.8) and experimental (T:Al = 1:6.6 and *syn:anti* = 13.6:1) results did not agree. The reasons why **2B** prefers activation of the 3° C–H bond will be described later in the discussion.

Interestingly, preferential activation of the 3° C–H bond by **2C** (Figure 3) is reminiscent of $\text{Ag}(\text{bpy})_2\text{OTf}$, previously reported to prefer 3° C–H over allylic C–H bond amination.^{17a} The resemblance between **2C** and $\text{Ag}(\text{bpy})_2\text{OTf}$ prompted us to investigate the TS of $[\text{Ag}(\text{bpy})_2\text{-nitrene(Al)}]^+$ (**2E**) for comparison. Indeed, TS-2C and TS-2E display similar

structures, where two pyridyl rings lie in the equatorial plane, one pyridyl ring is located in the axial position *trans* to the nitrene and a fourth ligand (a pyridyl ring in **TS-2C** and OTf^- anion in **TS-2E**) occupies the third position of a triangle in the equatorial plane. The steric congestion in the equatorial plane points the vinyl group away from the Ag, preventing its interaction with the alkene π electrons. This leads to preferred reaction of the 3° C–H bond over the allylic C–H bond for **2E** (calcd: T:Al = 5.2:1, *syn:anti* = 1.13:1; experiment: T:Al = 1.1:1, *syn:anti* = 3.7:1 (1,1-Me₂allylic C–H bond)).

The unexpected preference for reaction of the 3° C–H bond over the allylic C–H bonds of **2B** is attributed to the η^2 -binding mode of the nitrene to the electron-deficient Ag center upon dissociation of a pyridyl arm (Figure 3). This binding mode has been reported in low-coordinate Ag complexes, and is supported by a crystal structure of Ag–sulfonamide,³⁵ as well as calculated structures of Ag–nitrene complexes supported by tris(pyrazolyl)borate (Tp) ligands.³⁶ Ring strain is imposed on the 7-membered TS, disfavoring activation of the allylic C–H bonds. Combining these findings, we conclude that **2B** and **2C** do not agree as well with experiment as does **2A**, suggesting that similar OTf^- -free species are also the most important reactive species in benzylic (**1A**) and propargylic (**3A**) C–H amination.

Figure 4 shows the favored *pro-syn* and *pro-anti* RC-3A structures for propargylic (Pg) vs T C–H bond amination.

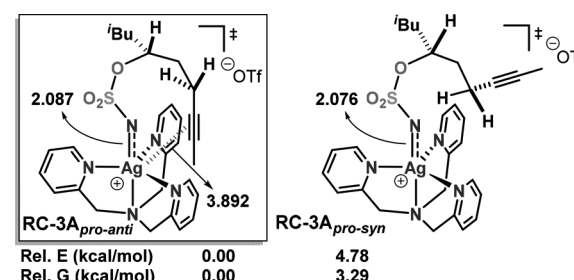


Figure 4. Reactant complex of Ag–nitrene complexes (nitrene = $\text{NSO}_3\text{-}(S)\text{-CH}(\text{iBu})(\text{Et-}(\text{C}\equiv\text{CMe}))$): RC-3A_{pro-anti} and RC-3A_{pro-syn}. Distances are shown in Å. Relative single point/Gibbs free energies are shown in kcal·mol⁻¹.

Calculations show that, despite an experimental *syn:anti* ratio of 3.1:1, only RC-3A_{anti} contains interactions between Ag and the ethynyl group at 3.89 Å. This interaction is absent in RC-3A_{syn} where the rigidity of the ethynyl group rotates it away from Ag when the *pro-syn* Pg C–H bond is proximal to the metal. The stabilizing Ag–ethynyl interaction lowers RC-3A_{anti} by 3.29 kcal·mol⁻¹ relative to RC-3A_{syn}. Stabilization of RC-3A_{anti} disfavors TS-3A_{syn} and TS-3A_{ter} under the Curtin–Hammett-corrected condition, decreasing the preference of **3A** for the *syn* product. This effect is less prominent in RC-1A ($\Delta G_{\text{anti}} < \Delta G_{\text{syn}}$ by 1.31 kcal·mol⁻¹) and RC-2A ($\Delta G_{\text{anti}} > \Delta G_{\text{syn}}$ by 0.23 kcal·mol⁻¹); hence, **1A** and **2A** display high *syn* dr. The Ag···π interaction between Ag and the ethynyl π electrons in **3A**_{anti} provides an excellent example of NCI-tuned regio- and diastereoselectivity, despite the fact that the interaction reduces dr by stabilizing the minor diastereomer.

Potential Energy Surfaces for Intramolecular NT by 1A, 2A, and 3A. To better understand the NT mechanism of $[\text{Ag}(\text{tpa})]^+$ and the driving force behind its regio- and stereoselectivities, DFT calculations were performed to study potential energy surfaces (PESs) for regioselective intra-

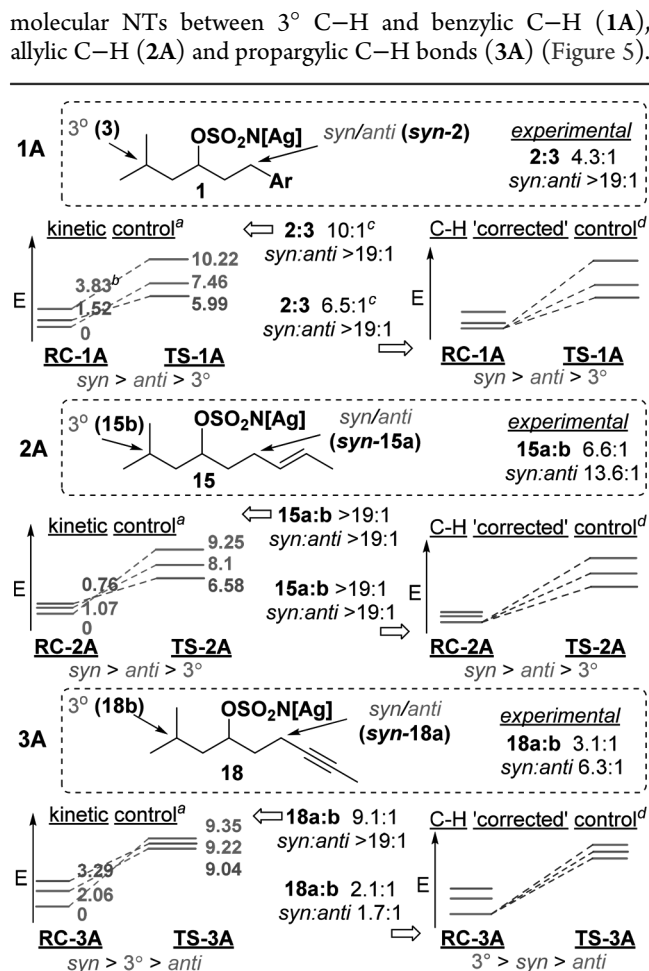


Figure 5. Kinetic-only controlled and Curtin–Hammett ‘corrected’ regio- and diastereoselectivities of 1–3A. (a) Product distribution calculated using eq 2 (see the SI). (b) Relative energies for Gibbs free energy with dispersion and solvent corrections in kcal mol⁻¹. (c) Selectivities were calculated without the D3 correction. (d) Product distribution calculated using eq 5 (see the SI).

In each case, RCs and TSs corresponding to 3° C–H insertion and the *syn* and *anti* diastereomers resulting from insertion at the α -conjugated C–H bond were considered. For RC and TS species, the triplet states are uniformly lower in energy; thus, only triplet states are shown in Figure 5. All PESs are similar in three ways: (1) NT proceeds on the triplet surface and spin crossover ensues after the TS (product-determining step, PDS), (2) the NT is initiated via initial H-atom transfer to the nitrene radical anion (both H^+ and e^- are accepted by nitrene \bullet^-) to yield an organic radical tethered to an Ag(II)tpa-amide species, and (3) the NT completes on the open-shell singlet (BS(1,1); broken-symmetry formalism) surface via radical recombination (RR) to produce the nitrene-inserted organic product and Ag(I)(tpa). The NT may proceed by (a) an elementary step with barrierless radical recombination occurring immediately after the HT, *E*-HT:RR or (b) a fast stepwise recombination, designated as an *S*-HT:RR mechanism. The distinguishing feature of *S*-HT:RR is that diradical intermediates are encountered on both the $^{BS(1,1)}\text{PES}$ (broken symmetry singlet with two antiferromagnetically coupled unpaired electrons) and ^3PES , whereas the *E*-HT:RR mechanism has an intermediate only on the ^3PES . NTs occurring via *E*-HT:RR give diastereospecific products, similar to Pérez’s³⁶ $[\text{Ag}(\text{Tp})]^+$ and

our previously reported $[\text{Ag}_2(\text{tpy})_2\text{OTf}]^+$ systems.^{16e} NTs that occur via *S*-HT:RR allow potential scrambling of diastereomers and radical inhibition when the resulting Ag(II)–amide complexes have a triplet ground state.^{17e,36}

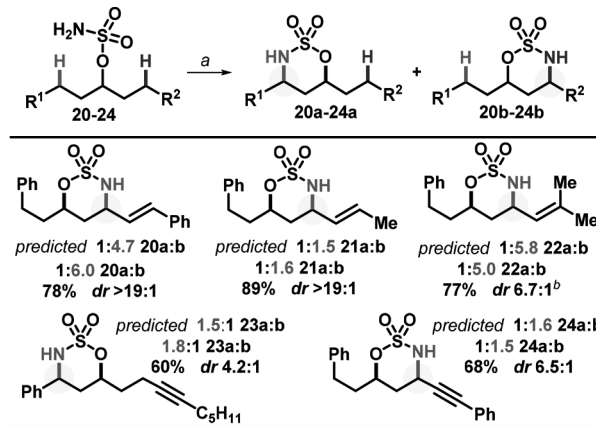
A look at the PESs for 1A, 2A, and 3A shows that, in each case, the energetic ordering of the RCs and TSs differs (Figure 5, e.g., *anti* < *syn* < 3° is observed for RC-1A, while the order is *syn* < *anti* < 3° for TS-1A). Thus, product selectivity can be governed solely through kinetic-only control or by a combination of kinetic and pre-equilibrium control (Curtin–Hammett ‘corrected’, see Figure S-1). The relative TS energetics were determined under both kinetic-only and Curtin–Hammett regimes. The selectivity pattern is identical for 1A and 2A; thus, we cannot distinguish whether the reactions proceed under kinetic-only or Curtin–Hammett-controlled control. For 1A, the energy ordering of the TSs is *syn* < *anti* < 3°, whether calculated from the lowest energy conformer of the RCs (SI, eq 5, Table S-16) or from their respective RC conformers (SI, eq 2). The calculated trend is consistent with experiment in that only the *syn* product is observed from benzylic C–H insertion and qualitatively consistent with experimental regioselectivity, despite overestimation of benzylic C–H activation. All three reactions proceed through the *E*-HT:RR mechanism to give the organic products after spin-crossover, with dr governed by the relative energy between TS-1A_{syn} and TS-1A_{anti} which translates to >20:1 dr (*syn:anti*), consistent with the experimentally observed dr. Similarly, the energy ordering of the TSs in the case of 2A is unaffected by the starting conformer of the RC; the trend is *syn* < *anti* < 3°, qualitatively consistent with the observed regioselectivity (Al:T = experimental 6.6:1 vs DFT > 19:1) and dr (*syn:anti* = expt 13.6:1 vs DFT 16.2:1) (Figure 5, Table S-19).

The propargylic case represented by 3A is very different from the benzylic and allylic cases denoted by 1A and 2A (Figure 5). Computed selectivities differ depending on whether they are calculated under kinetic-only (SI, eq 2; Table S-22) or Curtin–Hammett control (SI, eq 5). The trend is 3° < *syn* < *anti* using Curtin–Hammett control; in contrast, the trend is *syn* < 3° < *anti* under kinetic control. The dependence of the energy ordering of the TS on the RC conformation allows us to test the paradigm of the Curtin–Hammett principle as applied to Ag-catalyzed NT. Based on the former orderings of TS-3A, the calculated regioselectivity is 3°:propargylic = 1:2.1 (DFT) vs the 1:3.1 experimental value (using 18a:18b in Table 4 as a model for 3A) and the calculated dr is *syn:anti* = 1.7:1 (DFT) vs a *syn:anti* = 6.3:1 experimental ratio. In contrast, kinetic-only control gives calculated regioselectivity for 3°:propargylic of 1:6.5 (DFT) vs experimental = 1:3.1, while the predicted *syn:anti* = > 20:1 (DFT) compares to an experimental *syn:anti* = 6.3:1. Both models give calculated regioselectivities in reasonable agreement with experiment. However, dr is overestimated by the kinetic-only model, because the 7-membered *pro-anti* TS brings the alkynyl group in proximity to the catalyst, resulting in repulsive steric interactions. The unfavorable conformation enforced by the *pro-anti* TS is the reason for high *syn* dr in the case of 1A and 2A. On the other hand, *syn* dr for 3A is mitigated in the Curtin–Hammett-corrected model when the pre-TS equilibrium is considered; the *pro-anti* RC-3A posits the alkynyl group next to the Ag center, allowing attractive NCIs to direct NT into the *pro-anti* C–H bond (Figure 4). These results highlight the flexibility of

the Ag coordination sphere as a catalyst design principle in these complexes for site-selective NT.

Summarizing the computational results, we suggest that the active Ag–nitrene complexes exist in form A, counteranion-free, and η^4 -tpa (Figures 2–4). The key feature of the Ag complex in form A, compared to NT catalysts based on Rh, Ru, and Fe, is a less saturated coordination sphere with an open site located *cis* to the Ag–nitrene bond. This coordination environment, unique to Ag and other group 11 elements, allows sufficient space between pyridyl rings of the tpa ligand to interact with substrates when NCIs such as π -stacking are applicable, exemplified in 1 and 11–14 and 20–24 (Table 5).

Table 5. Predicted and Experimental Comparisons of Nitrene Transfer with Substrates Containing Competing NCIs



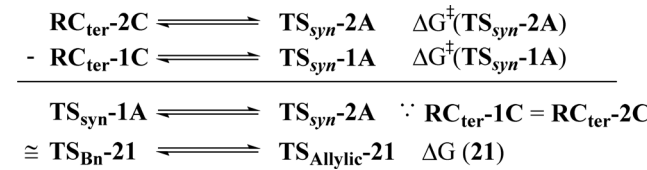
^a10 mol % of Ag(tpa)OTf, 3.5 equiv of PhIO, 0.05 M CHCl₃, 4 Å MS, –20 °C. ^b5% rearranged aziridination product.

vide infra). In addition, the fourth coordination site on Ag *cis* to the Ag–nitrene bond allows NCIs between π -electrons in substrates and the metal, as in 15–19 and 20–24. NCIs are thus important in tuning the energetics among TSs and different accessible reactant conformers, impacting the regioselectivity and dr of NTs promoted by Ag(tpa)OTf.

Predicting Selectivity between Competing α -Conjugated C–H Bonds. In addition to highlighting the potential for NCIs to drive selectivity in Ag-catalyzed NT, we explored if our experimental and computational data might be utilized to predict site-selectivity in new sets of substrates with competing α -conjugated C–H bonds (Table 5). Experimental predictions of product distributions with 20–24 were calculated in the following manner: the selectivities for each of the α -conjugated C–H bonds in 20–24 vs an isopropyl 3° alkyl C(sp³)–H bond were gleaned from Tables 1–4. The two numbers were divided to predict which α -conjugated C–H bond in 20–24 is favored. For example, to predict selectivity for 20 with Ag(tpa)OTf at –20 °C in CHCl₃, the selectivity for allylic C–H activation in 17 (>19:1, Table 4) is divided by that for benzylic C–H activation in 1 (4.3:1, Table 2) to give ~20/4.3 = 4.7:1. The experimental value for 20a:b is 6.0:1 (Table 3); an accurate match, given that the 17a:b ratio was measured by ¹H NMR. Extending this analysis to 21–24 gave predicted ratios for 21–24a:21–24b, close to experimental values. We anticipate that this simple model can be extended to NTs catalyzed by other metals.

This simple predictive model is based on a transition state equivalent to Hess's law (Scheme 3). The underlying

Scheme 3. Transition-State Hess's Law



assumption is that the potential energy surfaces for the isopropyl reference points are negligibly different (i.e., 1C–RC_{ter} ≈ 2C–RC_{ter}). For example, the selectivity in 21 and 23 is computationally modeled using the enthalpies and entropies of activation previously calculated for 1A_{Bn}, 2A_{Al}, and 3A_{Pg} relative to their corresponding RC_{ter}, similar to tabulated enthalpies and entropies of formation for molecules relative to the most stable form of the constituting elements. In this manner, regioselectivities for 21 and 23 can be estimated without computing entire potential energy surfaces for the nitrene complexes of 21 and 23, respectively (Table 6). This method is identical to the simple division procedure employed in Table 5.

Table 6. Calculated vs Experimental Regioselectivities and dr of 21 and 23 under Curtin–Hammett-Corrected (CH) Control

regiosomer (X)	calcd Bn:X ^a (expt)	calcd <i>syn:anti</i> (expt)
Al (21a:21b)	1:1.26 (1:1.6)	>19:1 (>19:1)
Pg (23a:23b)	1:1.53 (1.8:1)	1.7:1 (4.2:1)

^aSelectivities were calculated from the relative energy of TS-1A_{Bn} with respect to (wrt) RC-1C_{ter} and TS-2A_{Al} wrt RC-2C_{ter} for 21 and the relative energy of TS-1A_{Bn} wrt RC-1C_{ter} and TS-3A_{Al} wrt RC-3C_{ter} for 23.

"Attractive" vs Repulsive NCIs in Ligand-Tunable Ag-Catalyzed Regioselective NT. "Attractive" NCIs (namely, Ag– π and π – π interactions) are a complementary strategy to steric-driven, repulsive NCIs for tuning regioselectivity in metal-catalyzed NT. Both types of NCIs enable catalyst control over the NT, rather than substrate control dictated by differences in the BDEs of the targeted C–H bonds, for example. We have also demonstrated that while 2A and 2E share identical metal centers and similar donor ligands (Figure 3 for computations), the two catalysts display opposite regioselectivities in most cases.^{17a}

To further demonstrate the importance of attractive vs repulsive NCIs in impacting selectivity of NT, 1A and [Ag(tpa)(NSO₃-(R)-(iBu)(CH₂Cy))]⁺ (4A, Cy = cyclohexyl) (Figure 6) were compared experimentally and computationally. The three functional groups containing the abstracted γ C–H bonds (iPr and Bn in 1 and iPr and Cy in 4A) form a sterically similar triad to minimize interference from repulsive NCIs in our analysis. Steric values as measured by Tolman's cone angles are iPr, 160; Bn, 165; and Cy, 170;³⁷ Charton values are 0.76, 0.7, and 0.87 and Sterimol values 1.9, 1.9 and 1.9, respectively.³⁸ Despite having similar steric profiles, experimentally observed ratios of iPr:Bn and iPr:Cy are highly catalyst-dependent (1:2.8 and 1.4:1 for Ag(tpa)OTf, compared to inverted trends of 2.8:1 and 1:3.5 with Ag(tBu₂bpy)₂OTf, not shown).^{17a,39} This highlights the fact that Ag-catalyzed NT in these cases is not operating under substrate-controlled regioselectivity. Computationally, we predict an iPr:Bn ratio of 8.1:1 for 4A (with CH correction and without D3 correction for consistency with calculations on 1A), which is slightly

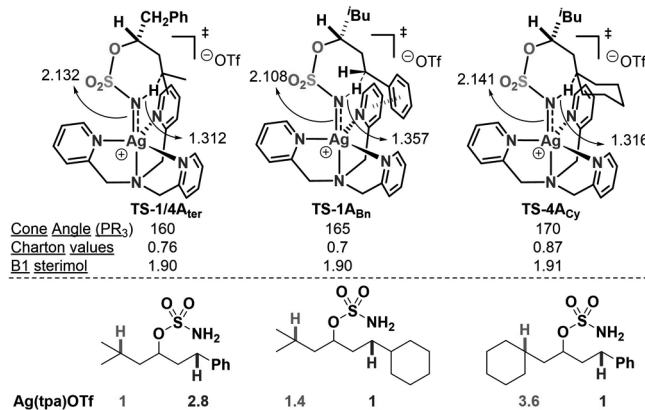


Figure 6. Ag–nitrene transition-state complexes: TS-1:4A_{ter}, TS-1A_{Bn}, and TS-4A_{ter}. Distances shown are in Å. Steric parameters are shown for proximal groups containing the abstracted C–H bond.

overestimated from the experimentally observed ratio of 1.4:1. **4A** contrasts with **1A** in terms of regioselectivity, despite the similar steric features of Bn and Cy. This mirrors the respective Ag–N and N···γH distances during the TS; breakage of the Ag–N bond occurs before formation of the N···γH bond begins in TS-4A_{ter} as compared to TS-4A_{Cy}, implying that approach of the Cy group is hindered in the TS. Elongation of the Ag–N bond, which increases the activation energy, is required to lessen the repulsive NCIs to access TS-4A_{Cy}. A different scenario is seen in **1A**, where TS-1A_{Bn} contains the longest N···γH bond, despite displaying the shortest Ag–N bond among the three TS structures in Figure 6. These bond features signal a very early transition state for TS-1A_{Bn} and rule out substrate-controlled regioselectivity for benzylic C–H abstraction (a more exothermic HAT and electron transfer are ruled out from the long N···γH bond and short Ag–N bond, respectively). This early TS is a result of preorganization of the TS structure due to attractive NCIs, further support that the Ag(tpa)⁺ catalyst operates via an overall attractive NCIs for **1A** vs repulsive NCIs for **4A**.

■ CONCLUSIONS

Intramolecular NT reactions catalyzed by Ag(tpa)OTf were found to be influenced by weak NCIs between the substrate and the catalyst. Experimentally, competitive amination was probed in a number of bifunctional substrates, including benzylic vs 3°, allylic vs 3°, propargylic vs 3°, benzylic vs allylic, and benzylic vs propargylic C–H bonds. Excellent yields and site-selectivities are observed in a number of cases, where contributions from NCIs are strongly implicated in determining the selectivity. These noncovalent interactions were probed computationally in detail. Both substrate aryl···tpa-pyridyl π···π interactions and Ag···π interactions were clearly observed in the lowest energy Ag–nitrene structures and transition states. We further showed how the experimentally determined selectivities and calculated transition states can be used to predict selectivities for new substrates that contain competing NCIs. These results set the stage for future catalyst developments that integrate noncovalent directing effects as a design element for group-transfer reactions. This strategy complements previous reliance on inherent steric and electronic features of reactive metal–nitrene intermediates to dictate selectivity.

■ ASSOCIATED CONTENT

■ Supporting Information

This material is available free of charge at The Supporting Information is available free of charge on the ACS Publications website at DOI: 10.1021/jacs.7b07619.

Experimental procedures (PDF)

NMR spectra (PDF)

Computational data (PDF)

Computational methods (PDF)

■ AUTHOR INFORMATION

Corresponding Authors

*berry@chem.wisc.edu

*schomakerj@chem.wisc.edu

ORCID

John F. Berry: 0000-0002-6805-0640

Jennifer M. Schomaker: 0000-0003-1329-950X

Author Contributions

[†]M.H. and T.Y. contributed equally.

Notes

The authors declare no competing financial interest.

■ ACKNOWLEDGMENTS

This work was funded through the Wisconsin Alumni Research Foundation (WARF) and NSF-1664374 to J.M.S. The NMR facilities at UW—Madison are funded by NSF (CHE-1048642, CHE-0342998) and NIH S10 OD012245. The NMR Facility at UW—Madison is supported by the NIH (P41GM103399, S10RR08438, S10RR029220) and NSF (BIR-0214394). J.F.B. thanks the Center for Selective C–H Functionalization supported by the NSF (CHE-1700982). The computational facility at UW—Madison is supported in part by NSF Grant No. CHE-0840494 and at the UW—Madison Center for High Throughput Computing (CHTC) in the Department of Computer Sciences. The CHTC is supported by UW—Madison, the Advanced Computing Initiative, the WARF, the Wisconsin Institutes for Discovery, and the NSF and is an active member of the Open Science Grid, which is supported by the NSF and the U.S. DOE Office of Science. U.S. Chimera is developed by the Resource for Biocomputing, Visualization, and Informatics at UCSF (supported by NIGMS P41-GM103311). Professor Robert Bergman is thanked for helpful comments and discussion.

■ REFERENCES

- (1) For selected references on directed C–H functionalization, see: (a) Rouquet, G.; Chatani, N. *Angew. Chem., Int. Ed.* **2013**, *52*, 11726. (b) Wang, C.; Huang, Y. *Synlett* **2013**, *24*, 145. (c) Rousseau, G.; Breit, B. *Angew. Chem., Int. Ed.* **2011**, *50*, 2450. (d) Song, G.; Wang, F.; Li, X. *Chem. Soc. Rev.* **2012**, *41*, 3651. (e) Yu, J.-Q.; Giri, R.; Chen, X. *Org. Biomol. Chem.* **2006**, *4*, 4041. (f) Patureau, F. W.; Glorius, F. *Angew. Chem., Int. Ed.* **2011**, *50*, 1977. (g) Engle, K. M.; Mei, T.-S.; Wasa, M.; Yu, J.-Q. *Acc. Chem. Res.* **2012**, *45*, 788. (h) Colby, D. A.; Tsai, A. S.; Bergman, R. G.; Ellman, J. A. *Acc. Chem. Res.* **2012**, *45*, 814. (i) Shul'pin, G. B. *Org. Biomol. Chem.* **2010**, *8*, 4217.

- (2) For selected references on nondirected C–H functionalization, see: (a) Das, S.; Incarvito, C. D.; Crabtree, R. H.; Brudvig, G. W. *Science* **2006**, *312*, 1941. (b) Crabtree, R. H. *J. Chem. Soc., Dalton Trans.* **2001**, *17*, 2437. (c) Hashiguchi, B. G.; Bischof, S. M.; Konnick, M. M.; Periana, R. A. *Acc. Chem. Res.* **2012**, *45*, 885. (d) Balcells, D.; Clot, E.; Eisenstein, O. *Chem. Rev.* **2010**, *110*, 749. (e) Kuhl, N.; Hopkinson, M. M.; Wencel-Delord, J.; Glorius, F. *Angew. Chem., Int.*

Ed. 2012, 51, 10236. (f) Arndtsen, B. A.; Bergman, R. G.; Mobley, T. A.; Peterson, T. H. *Acc. Chem. Res.* 1995, 28, 154. (g) Wencel-Delord, J.; Glorius, F. *Nat. Chem.* 2013, 5, 369. (h) Wencel-Delord, J.; Dröge, T.; Liu, F.; Glorius, F. *Chem. Soc. Rev.* 2011, 40, 4740. (i) Shul'pin, G. B. *Dalton Trans.* 2013, 42, 12794.

(3) References on synthesis and importance of amines, see: (a) Lawrence, S. A. *Amines: Synthesis, Properties and Applications*; Cambridge University Press: New York, 2004. (b) Nugent, T. C.; El-Shazly, M. *Adv. Synth. Catal.* 2010, 352, 753. (c) Smith, M. B. *Compendium of Organic Synthetic Methods*; Wiley, New York, 2009; Vol. 12. (d) Emerson, W. S. *The Preparation of Amines by Reductive Alkylation in Organic Reactions*; Wiley: New York, 2004. (e) Afagh, N. A.; Yudin, A. K. *Angew. Chem., Int. Ed.* 2010, 49, 262.

(4) Reviews on nitrene transfer: (a) Zalatan, D. N.; Du Bois, J. *Top. Curr. Chem.* 2009, 292, 347. (b) Muller, P.; Fruit, C. *Chem. Rev.* 2003, 103, 2905. (c) Li, Z. G.; He, C. *Eur. J. Org. Chem.* 2006, 2006, 4313. (d) Halfen, J. A. *Curr. Org. Chem.* 2005, 9, 657. (e) Dequirez, G.; Pons, V.; Dauban, P. *Angew. Chem., Int. Ed.* 2012, 51, 7384. (f) Collet, F.; Dodd, R. H.; Dauban, P. *Chem. Commun.* 2009, 34, 5061. (g) Collet, F.; Lescot, C.; Dauban, P. *Chem. Soc. Rev.* 2011, 40, 1926. (h) Degennaro, L.; Trinchera, P.; Luisi, R. *Chem. Rev.* 2014, 114, 7881.

(5) Selected reviews of Rh-catalyzed nitrene transfer: (a) Roizen, J. L.; Harvey, M. E.; Du Bois, J. *Acc. Chem. Res.* 2012, 45, 911. (b) Collet, F.; Lescot, C.; Liang, C. G.; Dauban, P. *Dalton Trans.* 2010, 39, 10401. For Ag, see: (c) Gómez-Emeterio, B. P.; Urbano, J.; Díaz-Requejo, M. M.; Pérez, P. J. *Organometallics* 2008, 27, 4126. (d) Kornecki, K. P.; Powers, D. C.; Ritter, T.; Berry, J. F. *Prog. Inorg. Chem.* 2014, 58, 225. (e) Kornecki, K. P.; Berry, J. F. *Chem. - Eur. J.* 2011, 17, 5827.

(6) For selected early examples of Ag-catalyzed nitrene transfer, see: (a) Cui, Y.; He, C. *J. Am. Chem. Soc.* 2003, 125, 16202. (b) Cui, Y.; He, C. *Angew. Chem., Int. Ed.* 2004, 43, 4210. (c) Li, Z.; Capretto, D. A.; Rahaman, R. H.; He, C. *Angew. Chem., Int. Ed.* 2007, 46, 5184. (d) Llaveria, J.; Beltran, A.; Diaz-Requejo, M. M.; Matheu, M. I.; Castillon, S.; Perez, P. J. *Angew. Chem., Int. Ed.* 2010, 49, 7092.

(7) Co/Pd-catalyzed nitrene transfer, see Huang, G. - H.; Li, J.-M.; Huang, J.-J.; Lin, J.-D.; Chuang, G. J. *Chem. - Eur. J.* 2014, 20, 5240.

(8) Selected examples of Ru-catalyzed nitrene transfer: (a) Au, S.-M.; Fung, W.-H.; Cheng, M.-C.; Che, C.-M.; Peng, S.-M. *Chem. Commun.* 1997, 1655. (b) Au, S.-M.; Huang, J.-S.; Che, C.-M.; Yu, W.-Y. *J. Org. Chem.* 2000, 65, 7858. (c) Harvey, M. E.; Musaev, D. G.; Du Bois, J. J. *Am. Chem. Soc.* 2011, 133, 17207. (d) Takaoka, A.; Moret, M.-E.; Peters, J. C. *J. Am. Chem. Soc.* 2012, 134, 6695. (e) Takaoka, A.; Gerber, L. C. H.; Peters, J. C. *Angew. Chem., Int. Ed.* 2010, 49, 4088. (f) Fantauzzi, S.; Gallo, E.; Caselli, A.; Ragaini, F.; Casati, N.; Macchi, P.; Cenini, S. *Chem. Commun.* 2009, 3952.

(9) For selected examples of Cu-catalyzed nitrene transfer, see: (a) Evans, D. A.; Faul, M. M.; Bilodeau, M. T. *J. Org. Chem.* 1991, 56, 6744. (b) Evans, D. A.; Faul, M. M.; Bilodeau, M. T. *J. Am. Chem. Soc.* 1994, 116, 2742. (c) Dielmann, F.; Andrade, D. M.; Frenking, G.; Bertrand, G. *J. Am. Chem. Soc.* 2014, 136, 3800.

(10) Selected references on Co-catalyzed nitrene transfer: (a) Lu, H. J.; Subbarayan, V.; Tao, J. R.; Zhang, X. P. *Organometallics* 2010, 29, 389–393. (b) Lu, H.-J.; Jiang, H.-L.; Hu, Y.; Wojtas, L.; Zhang, X. P. *Org. Lett.* 2012, 14, 5158–5161. (c) Lu, H.-J.; Jiang, H.-L.; Hu, Y.; Wojtas, L.; Zhang, X. P. *Chem. Sci.* 2011, 2, 2361–2366. (d) Lu, H.-J.; Jiang, H.-L.; Wojtas, L.; Zhang, X. P. *Angew. Chem., Int. Ed.* 2010, 49, 10192–10196. (e) Lu, H.-J.; Li, C.-Q.; Jiang, H.-L.; Lizardi, C. L.; Zhang, X. P. *Angew. Chem., Int. Ed.* 2014, 53, 7028–7032.

(11) For examples with Fe, see: (a) Kuppuswamy, S.; Powers, T. M.; Johnson, B. M.; Bezpalko, M. W.; Brozek, C. K.; Foxman, B. M.; Berben, L. A.; Thomas, C. M. *Inorg. Chem.* 2013, 52, 4802. (b) King, E. R.; Hennessy, E. T.; Betley, T. A. *J. Am. Chem. Soc.* 2011, 133, 4917. (c) Bowman, A. C.; Milsmann, C.; Bill, E.; Turner, Z. R.; Lobkovsky, E.; DeBeer, S.; Wieghardt, K.; Chirik, P. J. *J. Am. Chem. Soc.* 2011, 133, 17353.

(12) (a) Hayes, C. J.; Beavis, P. W.; Humphries, L. A. *Chem. Commun.* 2006, 4501. (b) Fiori, K. W.; Du Bois, J. J. *Am. Chem. Soc.* 2007, 129, 562. (c) Zalatan, D. N.; Du Bois, J. J. *Am. Chem. Soc.* 2008, 130, 9220. (d) Kornecki, K. P.; Berry, J. F. *Eur. J. Inorg. Chem.* 2012, 562. (e) Cramer, S. A.; Jenkins, D. M. *J. Am. Chem. Soc.* 2011, 133, 19342. (f) Hennessy, E. T.; Liu, R. Y.; Iovan, D. A.; Duncan, R. A.; Betley, T. A. *J. Am. Chem. Soc.* 2014, 5, 1526. (g) Srivastava, R. S.; Tarver, N. R.; Nicholas, K. M. *J. Am. Chem. Soc.* 2007, 129, 15250. (h) Barman, D. N.; Nicholas, K. M. *Eur. J. Org. Chem.* 2011, 2011, 908. (i) Davies, H. M. L.; Manning, J. R. *Nature* 2008, 451, 417. (j) Ramirez, T. A.; Zhao, B.; Shi, Y. *Chem. Soc. Rev.* 2012, 41, 931.

(13) Fiori, K. W.; Espino, C. G.; Brodsky, B. H.; Du Bois, J. *Tetrahedron* 2009, 65, 3042.

(14) Selected references: (a) Milo, A.; Neel, A. J.; Toste, F. D.; Sigman, M. S. *Science* 2015, 347, 737. (b) Krenske, E. H.; Houk, K. N. *Acc. Chem. Res.* 2013, 46, 979. (c) Knowles, R. R.; Jacobsen, E. N. *Proc. Natl. Acad. Sci. U. S. A.* 2010, 107, 20678. (d) Wheeler, S. E.; Bloom, J. W. G. *J. Phys. Chem. A* 2014, 118, 6133. (e) Houk, K. N.; Cheong, P. H.-Y. *Nature* 2008, 455, 309. (f) Neel, A. J.; Hilton, M. J.; Sigman, M. S.; Toste, F. D. *Nature* 2017, 543, 637. (g) Evans, D. A.; Faul, M. M.; Bilodeau, M. T. *J. Am. Chem. Soc.* 1994, 116, 2742. (h) Li, Z.; Conser, K. R.; Jacobsen, E. N. *J. Am. Chem. Soc.* 1993, 115, 5326.

(15) Olivos Suarez, A. I.; Jiang, H.; Zhang, X. P.; de Bruin, B. *Dalton Trans.* 2011, 40, 5697–5705 and references cited therein.

(16) (a) Hung-Low, F.; Renz, A.; Klausmeyer, K. K. *Polyhedron* 2009, 28, 407. (b) Hung-Low, F.; Renz, A.; Klausmeyer, K. K. *J. Chem. Crystallogr.* 2011, 41, 1174. (c) Du, J.; Hu, T.; Zhang, S.; Zeng, Y.; Bu, X. *CrystEngComm* 2008, 10, 1866. (d) Zhang, H.; Chen, L.; Song, H.; Zi, G. *Inorg. Chim. Acta* 2011, 366, 320. (e) Hung-Low, F.; Renz, A.; Klausmeyer, K. K. *J. Chem. Crystallogr.* 2009, 39, 438. (f) Levason, W.; Spicer, M. D. *Coord. Chem. Rev.* 1987, 76, 45. (g) Leschke, M.; Rheinwald, G.; Lang, H. Z. *Z. Anorg. Allg. Chem.* 2002, 628, 2470. (h) Zhu, H.-L.; Chen, Q.; Peng, W.-I.; Qi, S.-J.; Xu, A.-L.; Chen, X.-M. *Chin. J. Chem.* 2001, 19, 263. (i) Bowmaker, G. A.; Effendy; Marfuah, S.; Skelton, B. W.; White, A. H. *Inorg. Chim. Acta* 2005, 358, 4371. (j) Paramonov, S. E.; Kuzmina, N. P.; Troyanov, S. I. *Polyhedron* 2003, 22, 837. (k) Han, Z.; Wang, Y.; Wu, J.; Zhai, X. *Solid State Sci.* 2011, 13, 1560. (l) Yuan, L.; Qin, C.; Wang, X.; Li, Y.; Wang, E. *Dalton Trans.* 2009, 4169.

(17) (a) Alderson, J. A.; Phelps, A. M.; Scamp, R. J.; Dolan, N. S.; Schomaker, J. M. *J. Am. Chem. Soc.* 2014, 136, 16720. (b) Rigoli, J. W.; Weatherly, C. D.; Alderson, J. M.; Vo, B. T.; Schomaker, J. M. *J. Am. Chem. Soc.* 2013, 135, 17238. (c) Rigoli, J. W.; Weatherly, C. D.; Vo, V. T.; Neale, S.; Meis, A. R.; Schomaker, J. M. *Org. Lett.* 2013, 15, 290. (d) Scamp, R. J.; Rigoli, J. W.; Schomaker, J. M. *Pure Appl. Chem.* 2014, 86, 381. (e) Dolan, N. S.; Scamp, R. J.; Yang, T.; Berry, J. F.; Schomaker, J. M. *J. Am. Chem. Soc.* 2016, 138, 14658–14667. (f) Ju, M.; Weatherly, C. D.; Guzei, I. A.; Schomaker, J. M. *Angew. Chem., Int. Ed.* 2017, 56, 9944–9948. (g) Huang, M.; Corbin, J. R.; Dolan, N. S.; Fry, C. G.; Vinokur, A.; Guzei, I. A.; Schomaker, J. M. *Inorg. Chem.* 2017, 56, 6725–6733. (h) Alderson, J. M.; Schomaker, J. M. *Chem. - Eur. J.* 2017, 23, 8571–8576. (i) Weatherly, C. D.; Alderson, J. M.; Hein, J.; Berry, J. F.; Schomaker, J. M. *Organometallics* 2017, 36, 1649–1661. (j) Scamp, R. J.; Jirak, J. G.; Dolan, N.; Guzei, I.; Schomaker, J. M. *Org. Lett.* 2016, 18, 3014.

(18) (a) Kristyan, S.; Pulay, P. *Chem. Phys. Lett.* 1994, 229, 175. (b) Hobza, P.; Sponer, J.; Reschel, T. *J. Comput. Chem.* 1995, 16, 1315. (c) Perezjorda, J. M.; Becke, A. D. *Chem. Phys. Lett.* 1995, 233, 134. (d) Grimme, S.; Antony, J.; Schwabe, T.; Mück-Lichtenfeld, C. *Org. Biomol. Chem.* 2007, 5, 741.

(19) Bruice, T. C.; Lightstone, F. C. *Acc. Chem. Res.* 1999, 32, 127. (20) (a) Paradine, S. M.; White, M. C. *J. Am. Chem. Soc.* 2012, 134, 2036. (b) Paradine, S. M.; Griffin, J. R.; Zhao, J.; Petronico, A. L.; Miller, S. M.; White, M. C. *Nat. Chem.* 2015, 7, 987.

(21) (a) Zhang, X.; Xu, H.; Zhao, C. *J. Org. Chem.* 2014, 79, 9799. (b) Varela-Álvarez, A.; Yang, T.; Jennings, H.; Kornecki, K. P.; Macmillan, S. N.; Lancaster, K. M.; Mack, J. B. C.; Du Bois, J.; Berry, J. F.; Musaev, D. G. *J. Am. Chem. Soc.* 2016, 138, 2327.

(22) Hansch, C.; Leo, A.; Taft, R. W. *Chem. Rev.* 1991, 91, 165.

(23) (a) Kuijpers, P. F.; Tiekkink, M. J.; Breukelaar, W. B.; Broere, D. L. J.; van Leest, N. P.; van der Vlugt, J. I.; Reek, J. N. H.; de Bruin, B. *Chem. - Eur. J.* 2017, 23, 7945–7952. (b) Lyaskovskyy, V.; Suarez, A. I. O.; Lu, H.; Jiang, H.; Zhang, X. P.; de Bruin, B. *J. Am. Chem. Soc.* 2011,

133, 12264–12273. (c) Goswami, M.; Lyaskovskyy, V.; Domingos, S. R.; Buma, W. J.; Woutersen, S.; Troeppner, O.; Ivanovic-Burmazovic, I.; Lu, H.; Cui, X.; Zhang, X. P.; Reijerse, E. J.; DeBeer, S.; van Schooneveld, M. M.; Pfaff, F. F.; Ray, K.; de Bruin, B. *J. Am. Chem. Soc.* **2015**, *137*, 5468–5479.

(24) For selected references, see: (a) Sinnokrot, M. O.; Valeev, E. F.; Sherrill, C. D. *J. Am. Chem. Soc.* **2002**, *124*, 10887–10893. (b) Hunter, C. A.; Sanders, J. K. *J. Am. Chem. Soc.* **1990**, *112*, 5525–5534. (c) Cozzi, F.; Cinquini, M.; Annunziata, R.; Siegel, J. S. *J. Am. Chem. Soc.* **1993**, *115*, 5330–5331. (d) Burley, S. K.; Petsko, G. A. *Science* **1985**, *229*, 23. (e) Sheppard, T. J.; Petti, M. A.; Dougherty, D. A. *J. Am. Chem. Soc.* **1988**, *110*, 1983. (f) Sunner, J.; Nishizawa, K.; Kebarle, P. *J. Phys. Chem.* **1981**, *85*, 1814. (g) Kearney, P. C.; Mizoue, L. S.; Kumpf, R. A.; Forman, J. E.; McCurdy, A.; Dougherty, D. A. *J. Am. Chem. Soc.* **1993**, *115*, 9907. (h) Kumpf, R. A.; Dougherty, D. A. *Science* **1993**, *261*, 1708. (i) Dougherty, D. *Science* **1996**, *271*, 163.

(25) For selected references, see: (a) Martinez, C. R.; Iverson, B. L. *Chem. Sci.* **2012**, *3*, 2191. (b) Wheeler, S. E.; Houk, K. N. *Mol. Phys.* **2009**, *107*, 749. (c) Wheeler, S. E.; Houk, K. N. *J. Am. Chem. Soc.* **2009**, *131*, 3126. (d) Wheeler, S. E.; Houk, K. N. *J. Chem. Theory Comput.* **2009**, *5*, 2301. (e) Raju, R. K.; Bloom, J. W. G.; An, Y.; Wheeler, S. E. *ChemPhysChem* **2011**, *12*, 3116. (f) Bloom, J. W. G.; Wheeler, S. E. *Angew. Chem., Int. Ed.* **2011**, *50*, 7847. (g) Wheeler, S. E. *J. Am. Chem. Soc.* **2011**, *133*, 10262. (h) Wheeler, S. E. *Acc. Chem. Res.* **2013**, *46*, 1029.

(26) Janiak, C. *Dalton Trans.* **2000**, 3885.

(27) Selected references: (a) Dewar, M. J. S. *Bull. Soc. Chim. Fr.* **1951**, *18*, C79. (b) Winstein, S.; Lucas, H. J. *J. Am. Chem. Soc.* **1938**, *60*, 836. (c) Williams, C. M.; Mander, L. N. *Tetrahedron* **2001**, *57*, 425. (d) Cottam, J. R. A.; Steel, P. J. *J. Organomet. Chem.* **2006**, *691*, 2286.

(28) (a) Breault, G. A.; Hunter, C. A.; Mayers, P. C. *J. Am. Chem. Soc.* **1998**, *120*, 3402. (b) Cubberley, M. S.; Iverson, B. L. *J. Am. Chem. Soc.* **2001**, *123*, 7560. (c) Gutmann, V. *Coord. Chem. Rev.* **1976**, *18*, 225. (d) Hunter, C. A.; Lawson, K. R.; Perkins, J.; Urch, C. J. *J. Chem. Soc., Perkin Trans.* **2001**, *2*, 651.

(29) Reichardt, C.; Welton, T. *Solvents and Solvent Effects in Organic Chemistry*, 4th ed.; Wiley-VCH, 2011.

(30) Hunter, C.; Sanders, J. K. *J. Am. Chem. Soc.* **1990**, *112*, 5525.

(31) For selected references, see: (a) Cockcroft, S. L.; Hunter, C. A.; Lawson, K. R.; Perkins, J.; Urch, C. J. *J. Am. Chem. Soc.* **2005**, *127*, 8594. (b) Cozzi, F.; Ponzini, F.; Annunziata, R.; Cinquini, M.; Siegel, J. S. *Angew. Chem., Int. Ed. Engl.* **1995**, *34*, 1019. (c) Newcomb, L. F.; Gellman, S. H. *J. Am. Chem. Soc.* **1994**, *116*, 4993–4994. (d) Rashkin, M. J.; Waters, M. L. *J. Am. Chem. Soc.* **2002**, *124*, 1860–1861. (e) Cubberley, M. S.; Iverson, B. L. *J. Am. Chem. Soc.* **2001**, *123*, 7560–7563. (f) Lai, J. S.; Qu, J.; Kool, E. T. *Angew. Chem., Int. Ed.* **2003**, *42*, 5973–5977. (g) Zahn, A.; Brotschi, C.; Leumann, C. J. *Chem. - Eur. J.* **2005**, *11*, 2125–2129. (h) Hunter, C. A. *Angew. Chem., Int. Ed.* **2004**, *43*, 5310–5324.

(32) Maier, J. M.; Li, P.; Hwang, J.; Smith, M. D.; Shimizu, K. D. *J. Am. Chem. Soc.* **2015**, *137*, 8014.

(33) Grimme, S.; Hansen, A.; Brandenburg, J. G.; Bannwarth, C. *Chem. Rev.* **2016**, *116*, 5105.

(34) (a) Bruno, J.; Cole, J. C.; Edgington, P. R.; Kessler, M.; Macrae, C. F.; McCabe, P.; Pearson, J.; Taylor, R. *Acta Crystallogr., Sect. B: Struct. Sci.* **2002**, *58*, 389. (b) Cambridge Structural Database, accessed Feb 22, 2017.

(35) Zanvettor, N. T.; Abbehausen, J.; Lustri, W. R.; Cuin, A.; Masciocchi, N.; Corbi, P. P. *J. Mol. Struct.* **2015**, *1082*, 180.

(36) Maestre, L.; Sameera, W. M.; Díaz-Requejo, M. M.; Maseras, F.; Pérez, P. *J. Am. Chem. Soc.* **2013**, *135*, 1338.

(37) Tolman, C. A. *Chem. Rev.* **1977**, *77*, 313–348.

(38) (a) Charton, M. *J. Am. Chem. Soc.* **1975**, *97*, 1552–1556. (b) Charton, M. *J. Am. Chem. Soc.* **1975**, *97*, 3691–3693. (c) Charton, M. *J. Org. Chem.* **1976**, *41*, 2217–2220. (d) *Drug Design*; Ariens, E. J., ed.; Academic Press, 1976, 133. (e) *Biological Activity and Chemical Structure*; Buisman, J. A., Ed.; Elsevier, 1977; p 63. (f) *QSAR in Drug Dosing and Toxicology*; Hadzi, B.; Jerman-Blazic, B., Ed.; Elsevier, 1987; p 97. (g) *IUPAC Pesticide Chemistry*, Vol. 1; Miyamoto, J., Ed.; Pergamon, 1983; p 339.

(39) Corbin, J. R.; Schomaker, J. M. *Chem. Commun.* **2017**, *53*, 4346–4349.